Spectromicroscopy study of interfacial Co/NiO(001)

G. van der Laan,[1] N. D. Telling,[2] A. Potenza,[1] S. S. Dhesi,[1] and E. Arenholz[3]

[1]*Diamond Light Source, Chilton, Didcot, Oxfordshire OX11 0DE, United Kingdom*
[2]*Institute for Science and Technology in Medicine, Keele University, Stoke-on-Trent ST4 7QB, United Kingdom*
[3]*Advanced Light Source, Lawrence Berkeley National Laboratory, Berkeley, CA 94720*

(Dated: September 26, 2010)

Photoemission electron microscopy (PEEM) with linearly polarized x-rays is used to determine the orientation of antiferromagnetic domains by monitoring the relative peak intensities at the $3d$ transition metal L_2 absorption edge. In such an analysis the orientations of the x-ray polarization $\hat{\mathbf{E}}$ and magnetization $\hat{\mathbf{H}}$ with respect to the crystalline axes has to be taken into account. We address this problem by presenting a general expression of the angular dependence for both x-ray absorption spectroscopy and x-ray magnetic linear dichroism (XMLD) for arbitrary direction of $\hat{\mathbf{E}}$ and $\hat{\mathbf{H}}$ in the (001) cubic plane. In cubic symmetry the angular dependent XMLD is a linear combination of two spectra with different photon energy dependence, which reduces to one spectrum when $\hat{\mathbf{E}}$ or $\hat{\mathbf{H}}$ is along a high-symmetry axis. The angular dependent XMLD can be separated into an isotropic term, which is symmetric along $\hat{\mathbf{H}}$, and an anisotropic term, which depends on the orientation of the crystal axes. The anisotropic term has maximal intensity when $\hat{\mathbf{E}}$ and $\hat{\mathbf{H}}$ have equal but opposite angles with respect to the [100] direction. The Ni^{2+} L_2 edge has the peculiarity that the isotropic term vanishes, which means that the maximum in the XMLD intensity is observed not only for $\hat{\mathbf{E}} \parallel \hat{\mathbf{H}} \parallel [100]$ but also for ($\hat{\mathbf{E}} \parallel [110]$, $\hat{\mathbf{H}} \parallel [1\bar{1}0]$). We apply the angular dependent theory to determine the spin orientation near the Co/NiO(100) interface. The PEEM images show that the ferromagnetic Co moments and antiferromagnetic NiO moments are aligned perpendicular to each other. By rotating the sample with respect to the linear x-ray polarization we furthermore find that the perpendicular coupling with the ferromagnetic Co layer at the interface causes a canting of the antiferromagnetic Ni moments. This shows that taking into account the angular dependence of the XMLD in the detailed analysis of PEEM images leads to an accurate retrieval of the spin axes of the antiferromagnetic domains.

PACS numbers: 75.25.-j, 75.70.Cn , 78.70.Dm

I. INTRODUCTION

Optimizing the electronic and magnetic properties of layered magnetic heterostructures for specific applications is a daunting task for materials engineering. Characterization techniques employing the absorption and scattering of soft x rays have emerged as important and powerful tools for the study of heterostructures. In fact, soft x-ray magnetic dichroism—i.e., the difference in absorption based on the relative orientation of the x-ray polarization and magnetic axes of a system—is often employed for element-, valence-, and site-specific magnetometry providing very high spatial and temporal resolution.

X-ray magnetic circular dichroism (XMCD) combined with sum rules for the integrated intensities has been very successful in providing element-specific spin and orbital magnetic moments of a wide range of magnetic materials.[1–4] X-ray magnetic linear dichroism (XMLD) has since long been established as a probe to study antiferro- as well as ferro- and ferri-magnetic materials.[5–9] The calculated $L_{2,3}$ XMCD and XMLD spectra for localized $3d$ transition metal ions with different crystal-field strengths have been published by van der Laan and Thole.[10] For itinerant $3d$ metallic systems the line shape of the $L_{2,3}$ XMLD spectra have been explained using the effective exchange field splitting of the core hole.[11] Sum rules for XMLD have been derived, which relate the integrated intensity over the L_3 and L_2 edges to the expectation values of the charge quadrupole moment and the anisotropic spin-orbit interaction.[12] Although, the integrals in the case of XMLD are smaller than for XMCD, their study has provided important insights in the microscopic origin of the magnetocrystalline anisotropy.[13–16] Kuneš and Oppeneer[17] calculated a huge magnetocrystalline anisotropy of the XMLD spectra at the $L_{2,3}$ edges of cubic Fe, Co, and Ni metal, which showed an opposite sign along different high-symmetry quantization axes. The anisotropy in the XMLD of itinerant metals was explained using the model for the effective exchange field splitting of the core hole.[11] The sign reversal of the XMLD signal was observed in $LaFeO_3$[18] by Czekay *et al.* The large anisotropy in the XMLD was confirmed by multiplet structure calculations by taking properly into account the core-valence Coulomb and exchange interactions.[19,20] A large anisotropy in the XMLD was found experimentally at the Mn^{2+} $L_{2,3}$ edge in (Ga,Mn)As, in good agreement with atomic multiplet calculations.[19] Since the half filled $3d$ shell of Mn carries no orbital moment, the angular dependence can not be ascribed to the magnetocrystalline anisotropy and indeed the integrated intensities of the $L_{2,3}$ XMLD vanish. The calculations show indeed that the $3d$ spin-orbit interaction has little or no effect on the XMLD and also that the angular dependence disappears when the crystal-field

interaction is switched off. In x-ray absorption (XA) the electric-dipole selection rules restrict the set of final states that can be reached from the ground state, which leads to different transition probabilities from the exchange-split core levels to the t_{2g} and e_g crystal field split empty d states. Therefore, the anisotropic XMLD is a property of the cubic wave functions for the d states with respect to the spin quantization axis, hence its orientation with respect to the crystal axes is important[20].

Using vector magnet magnetometry[21] the full angular dependence of the XMLD has been investigated and compared to multiplet calculations for the transition metal $L_{2,3}$ edges of $Ga_{1-x}Mn_xAs$,[19] Fe_3O_4,[20] $NiFe_2O_4$, NiO,[22–24] $CoFe_2O_4$,[25], Co-based Heusler alloys,[26] $La_{0.7}Sr_{0.3}FeO_3$,[27] and Fe_xGa_{1-x},[15] and the rare earth $M_{4,5}$ edges of EuO.[28] It was found that the angular dependent XMLD could be described by a linear combination of two independent spectra, which we called fundamental spectra.[19,20]

For antiferromagnetic systems, the spin orientation has been studied using the linear polarization dependence of the intensity ratio of the two XA peaks at the L_2 edge. Alders *et al.*[29,30] have measured a NiO sample with a statistical distribution of $\langle\pm1\pm1\pm2\rangle$ possible spin directions. In their analysis, which is correct for axial symmetry, the spin orientation with respect to the crystallographic axes was not explicitly take into account. The same approach was used to analyze the antiferromagnetic domain structures of $LaFeO_3$[31–33] and NiO.[34–40] However, as was first demonstrated by Arenholz *et al.*,[22] for a correct interpretation of the XA spectra the relative orientation of $\hat{\mathbf{E}}$ and $\hat{\mathbf{H}}$ with respect to the crystal frame has to be taken into account. This has been applied in several recent studies of various NiO surfaces and interfaces.[23,24,41–44] To analyze the PEEM images of Fe_3O_4/NiO interfaces, Krug *et al.*[41] proposed a theoretical model in which the diagonal and non-diagonal elements have opposite sign. This model, which explains the L_2 edge behavior, gives two independent XA spectra, so that there is only one XMLD spectrum, which has opposite sign for $\hat{\mathbf{E}} \parallel \hat{\mathbf{H}} \parallel [100]$ and $\hat{\mathbf{E}} \parallel \hat{\mathbf{H}} \parallel [110]$. However, this contradicts the earlier results which showed that in cubic symmetry there are two independent XMLD spectra.[20] In this paper we will address this issue by presenting a general expression of the angular dependence for both XA and XMLD for arbitrary directions of $\hat{\mathbf{E}}$ and $\hat{\mathbf{H}}$ in the (001) cubic plane. We find that in cubic symmetry there are three independent XA spectra and two independent XMLD spectra.

A concise description of the angular dependence of the XMLD for NiO has been given in Ref. 22. Here, we will present a more detailed description of the theory which is generally valid for XMLD. An expression of the angular dependence for arbitrary direction of $\hat{\mathbf{E}}$ and $\hat{\mathbf{H}}$ in the (001) plane is given for both XA and XMLD. While the angular dependent XMLD is a linear combination of two fundamental spectra, this reduces to a single spectrum when either $\hat{\mathbf{E}}$ or $\hat{\mathbf{H}}$ is along a high-symmetry axis. Furthermore, we will show that the XMLD can be separated into a rotational invariant ("isotropic") and angular dependent ("anisotropic") term. The latter depends on the orientation of $\hat{\mathbf{E}}$ and $\hat{\mathbf{H}}$ with respect to the crystalline axes. The isotropic term is rigidly attached to the direction of $\hat{\mathbf{H}}$ with an intensity that is maximal when $\hat{\mathbf{E}}$ and $\hat{\mathbf{H}}$ are parallel. On the other hand, the anisotropic term has maximal intensity when $\hat{\mathbf{E}}$ and $\hat{\mathbf{H}}$ have equal but opposite angles to the [100] direction. The Ni^{2+} L_2 XMLD has the peculiarity that the isotropic term vanishes, so that it contains only an anisotropic term. This means that the maximum in the XMLD intensity is not only observed when $\hat{\mathbf{E}} \parallel \hat{\mathbf{H}} \parallel [100]$ but also when ($\hat{\mathbf{E}} \parallel [110]$, $\hat{\mathbf{H}} \parallel [1\bar{1}0]$). This illustrates that to determine the antiferromagnetic domain structure it is essential to take into account the orientation of $\hat{\mathbf{E}}$ and $\hat{\mathbf{H}}$ with respect to the crystalline axes. We apply the angular dependent theory to analyze the PEEM images of Co/NiO(001). It is found that the ferromagnetic (FM) Co moments and antiferromagnetic (AFM) NiO moments are aligned perpendicular to each other. Moreover, by rotating the sample with respect to the in-plane linear polarization we obtain evidence for a tilting of the Ni moments.

This paper is organized as follows. In Sec. II we treat the detailed theory of the angular dependent XA and XMLD spectra. In Sec. III we digress to summarize some general details about the domain structure of NiO. The experimental details are given in Sec. IV. The results are presented and discussed in Sec. V and the conclusions are given in Sec. VI.

II. THEORY

A. XMLD angular dependence

In this study we restrict ourselves specifically to the (001) plane in the cubic lattice symmetry. This simplifies the expressions for the XMLD angular dependence, yet it clearly reveals the dependence on the crystallographic axes and shows the details to be taken into account. Moreover, this plane is often studied experimentally.

The XMLD is taken as the difference between two XA spectra measured with different orientations of the x-ray linear polarization, $\hat{\mathbf{E}}$, and the local magnetic moment, $\hat{\mathbf{H}}$. Either $\hat{\mathbf{E}}$ or $\hat{\mathbf{H}}$ is rotated by 90° between two successive XA measurements. In the (001) plane we have

$$I_{\mathrm{XA}}^{\mathrm{av}} = \frac{1}{2}[I_{\mathrm{XA}}(\varepsilon,\mu) + I_{\mathrm{XA}}(\varepsilon,\mu+90^\circ)], \quad (1a)$$

$$I_{\mathrm{XMLD}}(\varepsilon,\mu) = I_{\mathrm{XA}}(\varepsilon,\mu) - I_{\mathrm{XA}}(\varepsilon,\mu+90^\circ), \quad (1b)$$

or vice versa

$$I_{\mathrm{XA}}(\varepsilon,\mu) = I_{\mathrm{XA}}^{\mathrm{av}} + \frac{1}{2}I_{\mathrm{XMLD}}(\varepsilon,\mu), \quad (2a)$$

$$I_{\mathrm{XA}}(\varepsilon,\mu+90^\circ) = I_{\mathrm{XA}}^{\mathrm{av}} - \frac{1}{2}I_{\mathrm{XMLD}}(\varepsilon,\mu), \quad (2b)$$

where ε and μ are the angles of $\hat{\mathbf{E}}$ and $\hat{\mathbf{H}}$, respectively, with respect to the [100] direction in the (001) plane. It can be verified that the average XA spectrum, $I_{\rm XA}^{\rm av}$, is independent of ε and μ.

To refer to the spectra for $\varepsilon = \mu = 0$, it will be useful to introduce the shorthand notation

$$I_{\parallel} \equiv I_{\rm XA}(\hat{\mathbf{E}} \parallel \hat{\mathbf{H}} \parallel [100]) = I_{\rm XA}^{\rm av} + \frac{1}{2} I_0, \tag{3a}$$

$$I_{\perp} \equiv I_{\rm XA}(\hat{\mathbf{E}} \parallel [010], \hat{\mathbf{H}} \parallel [100]) = I_{\rm XA}^{\rm av} - \frac{1}{2} I_0, \tag{3b}$$

with $I_{\rm XA}^{\rm av} = \frac{1}{2}(I_{\parallel} + I_{\perp})$ and $I_0 = I_{\parallel} - I_{\perp}$.

For electric-dipole transitions, which limits higher-order terms, the symmetry conditions for the square planer D_{4h} $(4/mmm)$ symmetry of the (001) lattice plane lead to an angular dependence

$$\begin{aligned} I_{\rm XMLD}(\varepsilon, \mu) &= I_0 \cos 2\varepsilon \cos 2\mu + I_{45} \sin 2\varepsilon \sin 2\mu \qquad (4a) \\ &= \frac{1}{2}(I_0 + I_{45}) \cos(2\varepsilon - 2\mu) \\ &\quad + \frac{1}{2}(I_0 - I_{45}) \cos(2\varepsilon + 2\mu), \qquad (4b) \end{aligned}$$

where I_0 and I_{45} are two independent spectra with different photon energy dependence, which we called fundamental spectra. The I_0 spectrum is obtained by setting $\varepsilon = \mu = 0°$ and the I_{45} spectra by setting $\varepsilon = \mu = 45°$. The angular dependence of XA spectra are immediately obtained by substitution of Eq. (4) into Eq. (2a).

The key expression, shown in Eq. (4), is a sum over terms with an angular and energy dependent factor. The symmetry imposes no restrictions on the values of the spectra I_0 and I_{45}, which are independent parameters. Rotating the sample by 45° about [001] exchanges I_0 and I_{45} in Eq. (4), which gives the [110] as the new reference direction of the crystal frame. The angular part is symmetric under exchange of μ and ε, and so are all equations derived from it. Consequently, a rotation of either $\hat{\mathbf{H}}$ or $\hat{\mathbf{E}}$ results in the same XMLD. Therefore, in the following it is sufficient to treat the case of varying ε at fixed μ, from which the result for varying μ at fixed ε will be evident. Note that the equivalence between $\hat{\mathbf{H}}$ or $\hat{\mathbf{E}}$ is no longer exact in a distorted cubic symmetry, where the $\langle 100 \rangle$ directions are different.[25]

The angular dependent XA contains three independent spectra, $I_{\rm XA}^{\rm av}$, I_0, and I_{45}, i.e., one more than the XMLD. It has found before that this result is generally valid for cubic symmetry in three dimensions.[20] The angular dependence of the XA and XMLD is shown in Fig. 1(a) and its decomposition into the terms with I_0 and I_{45} is shown in Fig. 1(b).

The complete angular dependence of the XMLD from a ferro- or ferrimagnet can be measured when it is possible to rotate $\hat{\mathbf{H}}$ using a sufficiently strong applied magnetic field. One way of doing this would be to take the difference between the XA spectra for $\hat{\mathbf{H}} \parallel \hat{\mathbf{E}}$ and $\hat{\mathbf{H}} \perp \hat{\mathbf{E}}$ and to rotate the sample about the [001] surface normal over the angle $\phi = \mu = \varepsilon$, which reduces Eq. (4) to

$$\begin{aligned} I_{\rm XMLD}(\phi) &= I_0 \cos^2 2\phi + I_{45} \sin^2 2\phi \\ &= \frac{1}{2}\left[I_0 + I_{45} + (I_0 - I_{45}) \cos 4\phi\right]. \qquad (5) \end{aligned}$$

In a PEEM experiment, one often encounters the situation that the local magnetization axis $\hat{\mathbf{H}}$ (sometimes called the spin axis) of a remanently magnetized domain is fixed at an angle μ_0, while the linear polarization direction is variable. For given angle μ_0 the XMLD in Eq. (4) has a maximum intensity $I_{\rm max}$ at $\varepsilon_{\rm max}$, which depends on the photon energy dependent intensities I_0 and I_{45} and is most easily obtained in numerical form. The angular dependence has the geometrical properties

$$I_{\rm XMLD}(\varepsilon_{\rm max}, \mu_0) \equiv I_{\rm XMLD}^{\rm max}, \tag{6a}$$

$$I_{\rm XMLD}(\varepsilon_{\rm max} \pm 45°, \mu_0) = 0, \tag{6b}$$

$$I_{\rm XMLD}(\varepsilon_{\rm max} \pm 90°, \mu_0) = -I_{\rm XMLD}^{\rm max}. \tag{6c}$$

Instead of measuring the XMLD, the magnetic contrast can also be obtained using the relative intensity of individual peaks in the XA spectrum that have a different linear polarization dependence. Comparing two images at different photon energies avoids the need to measure with different polarization or magnetization directions. We will employ this method in Sec. V.

B. XMLD along high-symmetry axes

From Eq. (4) it is clear that an analysis of the angular dependent XMLD requires some knowledge of the photon energy dependent intensities I_0 and I_{45}. However, the situation simplifies considerably if $\hat{\mathbf{H}}$ (or $\hat{\mathbf{E}}$) is aligned along a high-symmetry axis. We give here the case for fixed μ, but as mentioned the roles of μ and ε can be exchanged. Substitution of either $\mu = 0°$ or 45° into Eq. (4) leads to

$$I_{\rm XMLD}(\varepsilon, \mu = 0°) = I_0 \cos 2\varepsilon, \tag{7a}$$

$$I_{\rm XMLD}(\varepsilon, \mu = 45°) = I_{45} \sin 2\varepsilon, \tag{7b}$$

for arbitrary ε. We can combine these results as

$$I_{\rm XMLD}(\varepsilon, \mu_c) = I_{\mu_c} \cos\left(2\varepsilon - 2\mu_c\right), \tag{8}$$

where $\mu_c = 0°$ or 45°. Thus the XMLD reaches a maximum intensity I_{μ_c} for $\varepsilon = \mu_c$, and according to Eq. (6) vanishes for $\varepsilon = \mu_c \pm 45°$, and obtains opposite intensity $-I_{\mu_c}$ for $\varepsilon = \mu_c \pm 90°$.

At all values of μ other than multiples of 45° the $I_{\rm XMLD}$ contains contributions from both I_0 and I_{45}. Thus only in the special cases with $\hat{\mathbf{H}}$ along a high-symmetry axis, $\langle 100 \rangle$ or $\langle 110 \rangle$, one measures a single spectrum (I_0 or I_{45}, respectively), while the direction of $\hat{\mathbf{E}}$ does not affect the spectral shape of the XMLD but only its magnitude. Furthermore, only when $\hat{\mathbf{H}}$ is along a symmetry axis (quantization axis), the ε dependence is symmetric around this

axis. Thus in the frequently encountered case in which $\hat{\mathbf{H}}$ is along a high-symmetry axis the anisotropy in the XMLD remains hidden. In order to study the angular dependence, $\hat{\mathbf{H}}$ needs to be forced along a non-symmetry direction by an applied magnetic field.

C. Isotropic and anisotropic part of the XMLD

For a rotation of the sample about [001] over an angle ϕ, the XMLD can be written as a sum over a rotational invariant term, which is independent of the crystal axes, and a term which depends on the orientation with respect to the crystalline axes [c.f., Eq. (4b)].

The isotropic term, i.e., rotational invariant contribution,

$$I^{\rm iso}_{\rm XMLD}(\varepsilon,\mu) \equiv \frac{1}{2}(I_0 + I_{45})\cos(2\varepsilon - 2\mu), \qquad (9)$$

depends only the difference $|\varepsilon - \mu|$ of the angles between $\hat{\mathbf{E}}$ and $\hat{\mathbf{H}}$. The geometrical properties of this term are

$$I^{\rm iso}_{\rm XMLD}(\varepsilon = \mu) = I^{\rm max-iso}_{\rm XMLD}, \qquad (10a)$$
$$I^{\rm iso}_{\rm XMLD}(\varepsilon = \mu \pm 45^\circ) = 0, \qquad (10b)$$
$$I^{\rm iso}_{\rm XMLD}(\varepsilon = \mu \pm 90^\circ) = -I^{\rm max-iso}_{\rm XMLD}, \qquad (10c)$$

with $I^{\rm max-iso}_{\rm XMLD} = \frac{1}{2}(I_0 + I_{45})$, which shows that its angular distribution is rigidly fixed to the direction $\hat{\mathbf{H}}$. This term does not depend on the orientation of the crystal frame. Note that since the anisotropic term in the XMLD vanishes at $\varepsilon = \mu = 22.5^\circ$, we can directly measure the pure isotropic term.

The anisotropic term, i.e., rotational dependent contribution,

$$I^{\rm ani}_{\rm XMLD}(\varepsilon,\mu) \equiv \frac{1}{2}(I_0 - I_{45})\cos(2\varepsilon + 2\mu), \qquad (11)$$

depends on the directions of $\hat{\mathbf{E}}$ and $\hat{\mathbf{H}}$ with respect to the crystal axes. The anisotropic term has the geometrical properties

$$I^{\rm ani}_{\rm XMLD}(\varepsilon = -\mu) = I^{\rm max-ani}_{\rm XMLD}, \qquad (12a)$$
$$I^{\rm ani}_{\rm XMLD}(\varepsilon = -\mu \pm 45^\circ) = 0, \qquad (12b)$$
$$I^{\rm ani}_{\rm XMLD}(\varepsilon = -\mu \pm 90^\circ) = -I^{\rm max-ani}_{\rm XMLD}, \qquad (12c)$$

with $I^{\rm max-ani}_{\rm XMLD} = \frac{1}{2}(I_0 - I_{45})$. Under sample rotation this term shows a $\cos 4\phi$ dependence [c.f., Eq. (5)].

The decomposition of the angular dependent XMLD into isotropic and anisotropic terms is illustrated in Fig. 1(c). The conditions in Eqs. (10) and (12) hold for arbitrary ε, and not only for $\varepsilon_{\rm max}$ as in Eq. (6), and are therefore more general.

In the absence of crystal-field symmetry, $I_{45} = I_0$, so that the anisotropic term vanishes and the XMLD is obtained as $I_0\cos(2\varepsilon - 2\mu)$, which depends only on

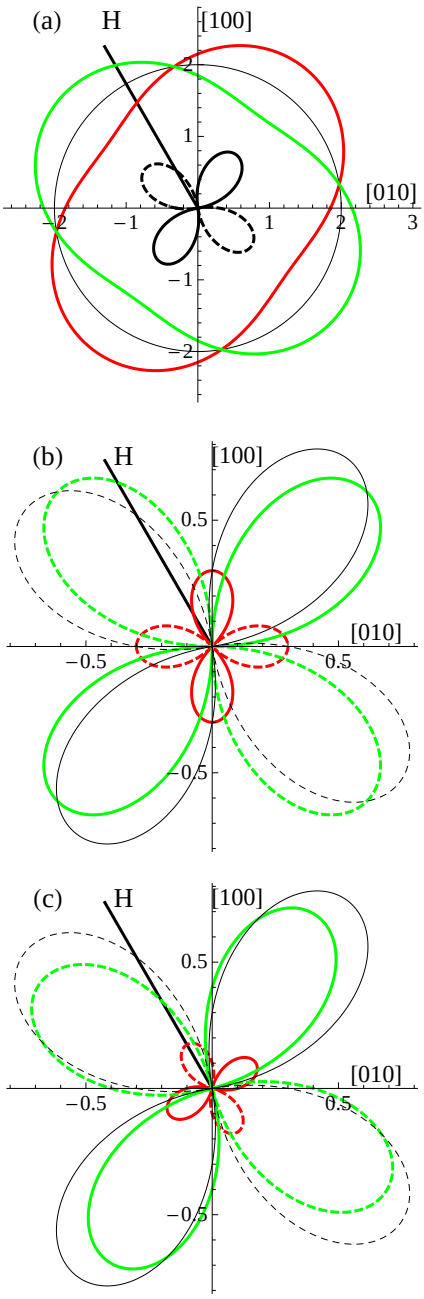

FIG. 1: (Color online) Polar plots of the XA and XMLD intensities in the (001) plane as a function of the angle ε for the linear polarization $\hat{\mathbf{E}}$ with fixed angle μ for the magnetization axis $\hat{\mathbf{H}}$ (indicated by the thick line) using Eq. (4) with the parameter values $I^{\rm av}_{\rm XA} = 2$, $I_0 = 0.6$, $I_{45} = -1$, and $\mu = -30^\circ$ with respect to the [100] crystal axis, which shows the effect of I_0 and I_{45} with opposite sign but not completely canceling each other. Drawn (dashed) lines correspond to positive (negative) intensities. (a) $I^{\rm av}_{\rm XA}$ (thin black line), $I_{\rm XA}(\varepsilon,\mu)$ [red (dark) line], $I_{\rm XA}(\varepsilon,\mu+90^\circ)$ [green (gray) line], and their intensity difference, $I_{\rm XMLD}(\varepsilon,\mu)$ (thick black line). (b) Decomposition of $I_{\rm XMLD}$ (thin black line) into contributions from I_0 [red (dark) line] and I_{45} [green (gray) line]. (c) Decomposition of $I_{\rm XMLD}$ (thin black line) into $I^{\rm iso}_{\rm XMLD}$ [red (dark) line] and $I^{\rm ani}_{\rm XMLD}$ [green (gray) line]. As seen the maximum of $I^{\rm iso}_{\rm XMLD}$ is along $\hat{\mathbf{H}}$, i.e., at $\varepsilon = \mu = -30^\circ$, whereas the maximum of $I^{\rm ani}_{\rm XMLD}$ is at $\varepsilon = -\mu = 30^\circ$.

the difference between the two angles. In order to retrieve the so-called "magic angle" results in cubic symmetry we have to use the alternative—but not equivalent—definition

$$I_{\mathrm{XMLD}}(\hat{\mathbf{E}},\hat{\mathbf{H}}) \equiv I_{\mathrm{XA}}(\hat{\mathbf{E}},\hat{\mathbf{H}}) - \frac{1}{2}\left[I_{\mathrm{XA}}(\hat{\mathbf{E}}_1,\hat{\mathbf{H}}) + I_{\mathrm{XA}}(\hat{\mathbf{E}}_2,\hat{\mathbf{H}})\right] = I_0\left[\frac{3}{2}\cos^2(\varepsilon-\mu) - \frac{1}{2}\right], \quad (13)$$

in which $\hat{\mathbf{E}}_1$ and $\hat{\mathbf{E}}_2$ are two mutual orthogonal vectors in the plane perpendicular to $\hat{\mathbf{E}}$. This provides for a rotational averaging in the perpendicular plane. The XMLD is maximal for $\varepsilon = \mu$, i.e., $\hat{\mathbf{H}} \parallel \hat{\mathbf{E}}$.[29]

The separation of the XMLD into anisotropic and anisotropic terms is particularly useful to describe the case where the crystal field is weak, so that the anisotropic term in the XMLD is small, i.e., $|I_0 - I_{45}| \ll |I_0 + I_{45}|$. For the Eu $M_{4,5}$ XMLD of ferromagnetic EuO, a small $I_0 - I_{45}$ spectrum could be extracted with a magnitude proportional to the effective crystalline electric field.[28] In the following we show that in the case of the Ni^{2+} L_2 edge only the anisotropic term gives a contribution.

D. Calculated Ni^{2+} $L_{2,3}$ edge spectra

Theoretical spectra were obtained using atomic multiplet calculations[10,45] for the electric-dipole transition Ni^{2+} $3d^8 \rightarrow 2p^5 3d^9$ in an octahedral crystal field of $10Dq = 1.4$ eV, which has a ground state $(t_2^6 e^2, {}^3A_2)T_2$. The Hartree-Fock values of the atomic Slater integrals (listed in Ref. 46) were scaled to 75% to account for interatomic screening and the $2p$ spin-orbit interaction was scaled to 98%. The obtained line spectra were convoluted with a Lorentzian of $\Gamma = 0.1$ (0.4) eV for the L_3 (L_2) edge to account for the intrinsic lifetime broadening and a Gaussian of $\sigma = 0.15$ eV for the instrumental broadening.

In the calculation the directions of the magnetization and x-ray polarization can be chosen in arbitrary directions. Multiplet calculations were performed with $\hat{\mathbf{E}}$ and $\hat{\mathbf{H}}$ separately incremented in steps of 5° over the full angular range. The results confirmed the angular relation in Eq. (4) to high accuracy, which shows that possible higher-order terms must be very small.

The calculated I_0 and I_{45} spectra are shown in Fig. 2(b), together with the resulting spectra for the isotropic and anisotropic terms, $\frac{1}{2}(I_0 + I_{45})$ and $\frac{1}{2}(I_0 - I_{45})$, respectively. For the entire L_2 edge as well as at the high energy side of the L_3 peak, $I_{45} \approx -I_0$. At energies just below the L_3 XA peak maximum we find $I_{45} \gg I_0$, while at energies just above it we find $I_{45} \approx I_0$. This demonstrates the presence of an isotropic term in the XMLD.

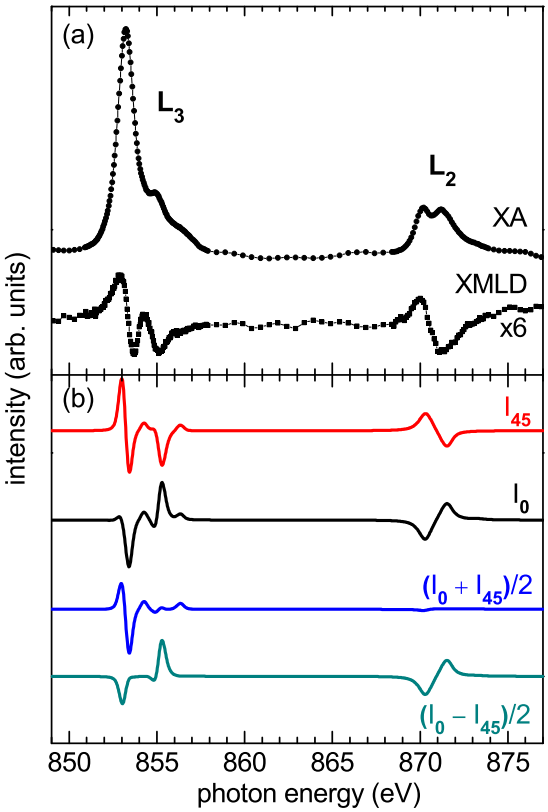

FIG. 2: (Color online) (a) Ni $L_{2,3}$ XA and XMLD measured as the difference between the two local XA spectra with in-plane linear x-ray polarization $\hat{\mathbf{E}} \parallel [110]$. (b) Multiplet calculations for the XMLD spectra I_{45} and I_0 and the isotropic and anisotropic terms $\frac{1}{2}(I_0 + I_{45})$ and $\frac{1}{2}(I_0 - I_{45})$, respectively.

E. Special case: Ni^{2+} L_2 edge

The equations for the angular dependence presented in the above are valid for the entire $L_{2,3}$ spectrum. If we restrict us to the Ni^{2+} L_2 edge a more specific rule can be derived.[22] This rule uses the fact that at this edge, $I_{45} \approx -I_0$, as can be verified from the calculation in Fig. 2(b). It should be noted that this relation is a peculiarity of the Ni^{2+} L_2 edge and is not true for the L_3 edge,[19,20] although it holds to some extend for other L_2 edges, such as for Co^{2+} (Ref. 25), Fe^{3+}, and Mn^{2+} (Ref. 19).

Substitution of $I_{45} = -I_0$ reduces Eq. (4) to

$$I_{\mathrm{XMLD}}^{L_2}(\varepsilon,\mu) = I_0 \cos(2\varepsilon + 2\mu). \quad (14)$$

This removes the isotropic term and retains only the anisotropic term. Therefore, the XMLD at the L_2 edge is strongly dependent on the orientation of $\hat{\mathbf{H}}$ and $\hat{\mathbf{E}}$ with respect to the crystal axes. Its geometrical properties are given by Eq. (12).

According to Eq. (14) the L_2 XMLD intensity is constant at its maximum of $\varepsilon = -\mu$. Since the total XMLD (isotropic and anisotropic terms) under this condition is

given by

$$I_{\mathrm{XMLD}}(\varepsilon=-\mu) = I_0\cos^2 2\mu - I_{45}\sin^2 2\mu, \qquad (15)$$

the L_3 XMLD will show a gradual change from I_0 for $\varepsilon=\mu=0^\circ$ to $-I_{45}$ for $\varepsilon=-\mu=45^\circ$. Both spectra are indistinguishable at the Ni^{2+} L_2 edge.

Instead of the XMLD, one can also use the intensity ratio, R_2, of the two peaks in the L_2 edge. Substitution of Eq. (14) with $I_0 \equiv I_\parallel - I_\perp$ into Eq. (2a) gives the angular dependence for the XA intensity,

$$\begin{aligned} I_{\mathrm{XA}}^{L_2}(\varepsilon,\mu) &= \frac{1}{2}\left[I_\parallel + I_\perp + (I_\parallel - I_\perp)\cos\left(2\varepsilon + 2\mu\right)\right] \\ &= I_\parallel\cos^2(\varepsilon+\mu) + I_\perp\sin^2(\varepsilon+\mu). \end{aligned} \qquad (16)$$

Note that for two peaks with different energies, the ratio R_2 will only show an approximate cosine square dependence, and this approximation will be better when the XMLD is small compared to the XA.

From Eq. (16) we obtain that $I_{\mathrm{XA}} = I_\parallel$ for $\varepsilon=-\mu$ and that $I_{\mathrm{XA}} = I_\perp$ for $\varepsilon=-\mu\pm 90^\circ$. From Eq. (2a) and spectra in Fig. 2(b) we find that the second peak in the L_2 edge is maximal for $I_\parallel$ and minimal for $I_\perp$.

The rules for XMLD in Eq. (14), or XA in Eq. (16), state that the maximal intensity is obtained when $\hat{\mathbf{H}}$ and $\hat{\mathbf{E}}$ have equal angles of opposite sign with respect to the [100] axis. Thus we obtain the maximal intensity $I_{\mathrm{XA}} = I_\parallel$ not only in the case of $\hat{\mathbf{E}} \parallel \hat{\mathbf{H}} \parallel [100]$ but also e.g., when $\hat{\mathbf{E}} \parallel [110], \hat{\mathbf{H}} \parallel [1\bar{1}0]$. In the latter case, $\hat{\mathbf{E}}$ and $\hat{\mathbf{H}}$ are aligned perpendicular to each other in the (001) plane.

III. DOMAIN STRUCTURE

A. Spin and domain wall orientations

The bulk magnetic structure of NiO below the Néel temperature ($T_N \approx 520$ K) consists of ferromagnetically aligned spins in $\langle 111\rangle$ planes, which are antiferromagnetically stacked with respect to each other. There are 24 different magnetic domains in total.[47–49] In bulk NiO four principal, so-called T(win) domains can be distinguished corresponding to the different $\langle 111\rangle$ orientations, i.e., [111], [11$\bar{1}$], [1$\bar{1}$1], and [$\bar{1}$11], which are denoted as T_1, T_2, T_3, and T_4, respectively. Each of these domains can be further divided into three S(pin) domains corresponding to the three possible $\langle 112\rangle$ directions with two different spin directions.[24,35,50] The domain walls are $\langle 110\rangle$ oriented. It was shown by Ohldag *et al.*[36] that for Co/NiO(001) the antiferromagnetic spins at the NiO interface are rotated in the (001) plane. Therefore, in the (001) plane the spin axis is along [110] for the $T_{1,2}$ domains and along [1$\bar{1}$0] for the $T_{3,4}$ domains. A picture of the lattice directions is shown in Fig. 3(a) The two sets of distinguishable domains have their domain walls along [100] and [010].[37]

IV. EXPERIMENTAL

A Co film of 2.5 nm thickness was grown by e-beam evaporation at room temperature under UHV conditions onto a freshly cleaved NiO(001) single crystal surface, following a recipe described in Ref. 37, and was capped with 1 nm Pd to prevent oxidation.

We employed photoemission electron microscopy (PEEM) to study the domain structure of AFM NiO using XMLD at the Ni $L_{2,3}$ edges. Domain images were acquired with an Elmitec PEEM[51] on the nanoscience beamline, I06, at the Diamond Light Source, UK. The beamline source is a pair of Apple II undulators working in the soft x-ray regime that can produce left and right circularly and linearly polarized x-rays. A plane grating monochromator provides a resolving power of up to 10,000 and a pair of Kirkpatrick–Baez mirrors focus the x-ray light to illuminate a 10 μm diameter spot on the sample.

The spatial variation of the XA coefficient was measured with a spatial resolution of ∼100 nm. The 100% linearly polarized x-rays impinged on the sample at a grazing angle of 16° and the linear polarization axis was in the plane of measurements. AFM NiO contrast was obtained by taking the ratio of two PEEM images obtained at the two most pronounced features of the Ni L_2 edge at 870 eV and 871 eV (spectra shown in Fig. 2). The linear polarization $\hat{\mathbf{E}}$ was oriented in the (001) interface plane and the crystal could be rotated about the [001] axis. The PEEM images with 15 μm field-of-view taken at the Ni L_2 are shown in Fig. 3. Stöhr *et al.*[34] have shown that the observed contrast is of magnetic origin since it disappears at the NiO Néel temperature. FM Co contrast was obtained by taking the ratio of two PEEM images obtained at the maximum of the L_3 and L_2 using circularly polarization, which measures the projection of the local magnetization onto the helicity vector, which is parallel to the x-ray beam.

V. RESULTS AND DISCUSSION

The PEEM images observed at photon energies 870 eV and 871 eV are denoted as A_1 and A_2, respectively. Figure 3(b) and (d) show the difference, $A_1 - A_2$, with ε at ∼45° and ∼22.5°, respectively. The magnetic contrast is clearly visible. For comparison, Fig. 3(c) shows the sum, $A_1 + A_2$, which is not sensitive to the magnetization. Very prominently visible in the magnetic contrast are the domain boundaries, which are along [100] and [010]. For reference the lattice directions for Fig. 3(b) are shown in Fig. 3(a).

Using the theory of the angular dependent XMLD for the (001) plane, described in Sec. II, allows us to distinguish between the domains with AFM axis oriented along [110] and [1$\bar{1}$0], i.e., with angles $\mu = 45^\circ$ and -45°, respectively. The sign of the XMLD intensity, which reverses when $\hat{\mathbf{E}}$ is rotated by 90°, reveals whether the spin

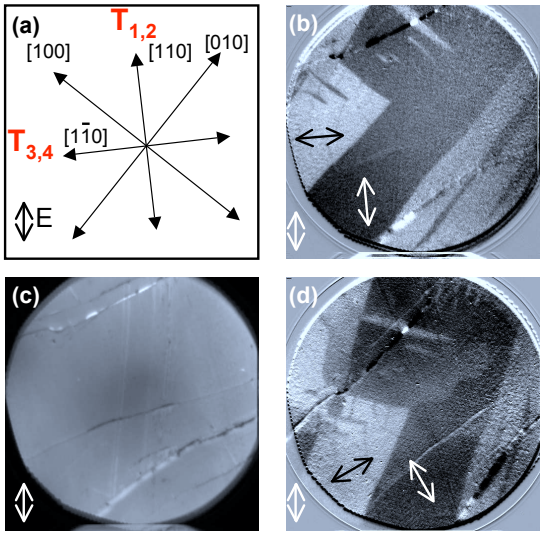

FIG. 3: (Color online) PEEM images with field-of-view = 15 μm for Co/NiO(001) measured at the Ni L_2 edge. (a) Lattice directions in the (001) interface plane before sample rotation, (b) difference, $A_1 - A_2$, (c) sum, $A_1 + A_2$, (d) difference, $A_1 - A_2$, with the sample rotated anticlockwise by $\sim$22.5°. A_1 and A_2 are the images taken at photon energies of 870 eV and 871 eV, respectively. The domain boundaries, which are along the [100] and [010] directions, are clearly visible. The linear x-ray polarization $\hat{\mathbf{E}}$ (double headed arrow in the lower left corner of each panel) in (b) is at $\varepsilon = 45°$, i.e., along [110], neglecting a mismatch angle of $\sim$5°. In the light (dark) areas the second peak of the L_2 edge is higher (lower), as in the $I_\parallel$ ($I_\perp$) spectrum, which means $\mu = -\varepsilon$ ($-\varepsilon \pm 90°$). Hence, the light (dark) areas have the spin axis at $\mu = -45°$ (45°), i.e., along the [1$\bar{1}$0] ([110]) direction (shown by double headed arrows), which correspond to the $T_{3,4}$ ($T_{1,2}$) domains.

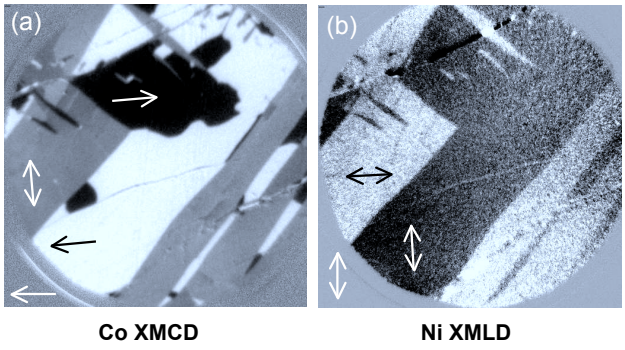

FIG. 4: PEEM images of Co/NiO(001) with field-of-view = 15 μm. (a) Ferromagnetic Co domains measured with circular polarization and (b) antiferromagnetic NiO domains measured with linear polarization. The polarization direction is indicated by the arrow in the bottom left corner of each panel. The other arrows indicate the spin directions of different domains. In the Co XMCD PEEM image the light and dark areas have the spin parallel and antiparallel to the light helicity vector, respectively. The gray areas in the Co image have the spin perpendicular to the light helicity. In the Ni XMLD PEEM image the light and dark areas have their spin axis along [1$\bar{1}$0] and [110], respectively, as in Fig. 3(b). This means that the ferromagnetic Co and antiferromagnetic NiO layers are coupled perpendicular.

axes of the domains are parallel or perpendicular to $\hat{\mathbf{E}}$.

Since the possible spin axes of the NiO(001) interface are at $\mu = \pm 45°$, only the I_{45} spectrum will be observed, regardless of the direction of $\hat{\mathbf{E}}$. We verified that we indeed measure the I_{45} and not the I_0 spectrum. Figure 2(a) shows the measured XA and XMLD spectra. The L_3 edge allows us to distinguish between I_0 and $-I_{45}$. Comparison with the calculated spectra in Fig. 2(b) shows a good agreement with the I_{45} spectrum.

In the light areas of the PEEM images the second peak of the L_2 edge is higher, as is the case in the $I_\parallel = I^{\rm av}_{\rm XA} + \frac{1}{2}I_0$ spectrum, which means according to Eq. (16) that $\mu = -\varepsilon$. Likewise, in the dark areas the second peak of the L_2 edge is lower, as is the case in the $I_\perp = I^{\rm av}_{\rm XA} - \frac{1}{2}I_0$ spectrum, which means $\mu = -\varepsilon \pm 90°$. Hence in Fig. 3(b), where $\varepsilon \approx 45°$, the light and dark areas have their spin axes along the [1$\bar{1}$0] and [110] directions, respectively, which correspond to $T_{3,4}$ and $T_{1,2}$ domains.

In Fig. 4 we compare PEEM images of the FM Co and AFM NiO domains for the same region of the Co/NiO(001) sample. The Co image was taken using XMCD with the helicity vector along [1$\bar{1}$0]. The spin directions are indicated by arrows. The light and dark areas in the Co image have the spin direction parallel and antiparallel to the x-ray helicity vector, respectively. The grey areas in the Co image have the spin perpendicular to the x-ray helicity vector. The dark areas in the NiO image are split into light and dark areas in the Co image. It is seen that the light areas in the NiO image correspond with grey areas in the Co image. Therefore, as reported previously,[22,23] the coupling between the Co and NiO spins is perpendicular at the interface.

In Fig. 3(d) the Co/NiO(001) sample is rotated counterclockwise by $\sim$22.5° compared to Fig. 3(b). As seen the AFM NiO domain structure remains the same in the rotated image. However, an additional faint contrast appears within the light and dark areas. In order to assign this, we compare the AFM NiO image in Fig. 3(d) with the FM Co XMCD image in Fig. 4(a). It is seen that there is a perfect match between the Co areas and the faint areas in the NiO at $\varepsilon \approx 22.5°$.

As explanation we suggest that the spin axes of the interface domains with nominal orientations along [110] and [1$\bar{1}$0] can be tilted towards either the [100] or [010] directions. For instance, for the $T_{1,2}$ domain the spin axis, $\hat{\mathbf{H}}$, is then along $\mu_1 = 45° - \tau$ or $\mu_2 = 45° + \tau$, where τ is the tilt angle.

The contrast between the areas with opposite tilt directions within $T_{1,2}$ is obtained using Eq. (4) as

$$I(\varepsilon, \mu_1) - I(\varepsilon, \mu_2) = 2I_0 \cos 2\varepsilon \sin 2\tau. \qquad (17)$$

This gives a τ dependence of the different areas in $T_{1,2}$ and $T_{3,4}$ for $\varepsilon = 45°$ and 0° as shown in Table I. Thus within each domain the difference in contrast is zero at

TABLE I: Tilt angle τ dependence of the different areas in the $T_{1,2}$ and $T_{3,4}$ domains for $\varepsilon = 45°$ and $0°$ (angle of $\hat{\mathbf{E}}$ with respect to [100]).

domains	spin axis	$\varepsilon = 45°$	$\varepsilon = 0°$
$T_{1,2}$	$[110]$ $\pm\tau$	$I_{45}\cos 2\tau$	$\pm I_0 \sin 2\tau$
$T_{3,4}$	$[1\bar{1}0]$ $\pm\tau$	$-I_{45}\cos 2\tau$	$\mp I_0 \sin 2\tau$

$\varepsilon = 45°$, while it is maximal at $\varepsilon = 0°$, with each domain splitting up into two different areas.

VI. CONCLUSIONS

We have studied antiferromagnetic NiO at the Co/NiO(001) interface using spectromicroscopy taking explicitly into account the strong dependence of the XMLD on the orientation of the linear light polarization, $\hat{\mathbf{E}}$, and the magnetic domain direction, $\hat{\mathbf{H}}$, with respect to the crystallographic axes.[20] In the past, the orientation of the Ni moments has been determined under the assumption that if the second peak in the L_2 absorption edge is maximal, then $\hat{\mathbf{H}} \parallel \hat{\mathbf{E}}$, which would be correct when there is only one fundamental spectrum. However, as was recently found,[22] a proper description of the angular dependent XMLD in cubic symmetry requires a linear combination of two fundamental spectra, I_0 and I_{45}. Taking into account the angular dependence, two extreme cases occur in the (001) plane: For $\hat{\mathbf{H}} \parallel \langle 100\rangle$ the XMLD is pure I_0 and for $\hat{\mathbf{H}} \parallel \langle 110\rangle$ the XMLD is pure I_{45}. While at the L_3 structure the I_0 and I_{45} spectra are distinctly different, the multiplet calculations for the Ni^{2+} L_2 edge show that $I_{45} \approx -I_0$. The L_2 absorption edge consists of a double peak structure which is often used for studying the spin orientation. The relation $I_{45} \approx -I_0$ means that the second peak is maximal not only for $\hat{\mathbf{E}} \parallel \hat{\mathbf{H}} \parallel \langle 100\rangle$ but also for $\hat{\mathbf{E}} \perp \hat{\mathbf{H}} \parallel \langle 110\rangle$. While in the latter case the moments are perpendicular instead of parallel to $\hat{\mathbf{E}}$, both orientations give the same Ni^{2+} L_2 XA spectrum. It is therefore essential in the analysis of PEEM images to take into account the angular dependence of the XMLD in order to retrieve the spin axes of the antiferromagnetic NiO domains.

Comparison with the Co XMCD PEEM images show that the spins of the ferromagnetic Co layer are aligned perpendicular to the NiO moments, as previously reported. However, we furthermore find that the perpendicular coupling induces a canting of the Ni moments, which can be observed as a splitting of the NiO domain contrast. As possible explanation we suggest that uncompensated Ni moments at the interface contribute to a tilt mechanism. It is known from XMCD measurements that there are uncompensated Ni moments near the interface oriented parallel to the Co moments. The Ni moments in NiO prefer to be oriented perpendicular to the Co and antiparallel to each other, and presumably, to the uncompensated Ni moments at the interface. The interplay of the two interactions—perpendicular to Co versus antiparallel to the uncompensated Ni moments—can lead to a component of the moments in the NiO collinear to the Co.

Acknowledgments

We acknowledge Diamond Light Source Ltd. for beamtime allocation on I06 under Proposal Reference SI545.

[1] B. T. Thole, P. Carra, F. Sette, and G. van der Laan, Phys. Rev. Lett. **68**, 1943 (1992).
[2] P. Carra, B. T. Thole, M. Altarelli, and X. Wang, Phys. Rev. Lett. **70**, 694 (1993).
[3] D. Weller, J. Stöhr, R. Nakajima, A. Carl, M. G. Samant, C. Chappert, R. Mégy, P. Beauvillain, P. Veillet, and G. A. Held, Phys. Rev. Lett. **75**, 3752 (1995).
[4] H. A. Dürr, G. van der Laan, and B. T. Thole, Phys. Rev. Lett. **76**, 3464 (1996).
[5] B. T. Thole, G. van der Laan, and G. A. Sawatzky, Phys. Rev. Lett. **55**, 2086 (1985).
[6] G. van der Laan, B. T. Thole, G. A. Sawatzky, J. B. Goedkoop, J. C. Fuggle, J.-M. Esteva, R. Karnatak, J. P. Remeika, and H. A. Dabkowska, Phys. Rev. B **34**, 6529 (1986).
[7] P. Kuiper, B. G. Searle, P. Rudolf, L. H. Tjeng, and C. T. Chen, Phys. Rev. Lett. **70**, 1549 (1993).
[8] M. M. Schwickert, G. Y. Guo, M. A. Tomaz, W. L. O'Brien, and G. R. Harp, Phys. Rev. B **58**, R4289 (1998).
[9] J. B. Kortright and S.-K. Kim, Phys. Rev. B **62**, 12216 (2000).
[10] G. van der Laan and B. T. Thole, Phys. Rev. B **43**, 13401 (1991).
[11] G. van der Laan, Phys. Rev. B **55**, 8086 (1997).
[12] G. van der Laan, Phys. Rev. Lett. **82**, 640 (1999).
[13] S. S. Dhesi, G. van der Laan, E. Dudzik, and A. B. Shick, Phys. Rev. Lett. **87**, 67201 (2001).
[14] S. S. Dhesi, G. van der Laan, and E. Dudzik, Appl. Phys. Lett. **80**, 1613 (2002).
[15] E. Arenholz, G. van der Laan, A. McClure, and Y. Idzerda, Phys. Rev. B **xx**, xxxxxx (2010).
[16] G. van der Laan, J. Phys.:Condens. Matter **10**, 3239 (1998).
[17] J. Kuneš and P. M. Oppeneer, Phys. Rev. B **67**, 024431 (2003).
[18] S. Czekaj, F. Nolting, L. J. Heyderman, P. R. Willmott, and G. van der Laan, Phys. Rev. B **73**, 020401 (2006).
[19] A. A. Freeman, K. W. Edmonds, G. van der Laan, N. R. S. Farley, T. K. Johal, E. Arenholz, R. P. Campion, C. T. Foxon, and B. L. Gallagher, Phys. Rev. B **73**, 233303 (2006).
[20] E. Arenholz, G. van der Laan, R. V. Chopdekar, and Y. Suzuki, Phys. Rev. B **74**, 094407 (2006).
[21] E. Arenholz and S. O. Prestemon, Rev. Sci. Instrum. **76**,

083908 (2005).
[22] E. Arenholz, G. van der Laan, R. V. Chopdekar, and Y. Suzuki, Phys. Rev. Lett. **98**, 197201 (2007).
[23] E. Arenholz, G. van der Laan, and F. Nolting, Appl. Phys. Lett. **93**, 162506 (2008).
[24] H. Ohldag, G. van der Laan, and E. Arenholz, Phys. Rev. B **79**, 052403 (2009).
[25] G. van der Laan, E. Arenholz, R. V. Chopdekar, and Y. Suzuki, Phys. Rev. B **77**, 064407 (2008).
[26] N. D. Telling, P. S. Keatley, G. van der Laan, R. J. Hicken, E. Arenholz, Y. Sakuraba, M. Oogane, Y. Ando, K. Takanashi, A. Sakuma, et al., Phys. Rev. B **78**, 184438 (2008).
[27] E. Arenholz, G. van der Laan, F. Yang, N. Kemik, M. D. Biegalski, H. M. Christen, and Y. Takamura, Appl. Phys. Lett. **94**, 072503 (2009).
[28] G. van der Laan, E. Arenholz, A. Schmehl, and D. G. Schlom, Phys. Rev. Lett. **100**, 067403 (2008).
[29] D. Alders, J. Vogel, C. Levelut, S. D. Peacor, T. Hibma, M. Sacchi, L. H. Tjeng, C. T. Chen, G. van der Laan, B. T. Thole, et al., Europhys. Lett. **32**, 259 (1995).
[30] D. Alders, L. H. Tjeng, F. C. Voogt, T. Hibma, G. A. Sawatzky, C. T. Chen, J. Vogel, M. Sacchi, and S. Iacobucci, Phys. Rev. B **57**, 11623 (1998).
[31] A. Scholl, J. Stöhr, J. Lüning, J. W. Seo, J. Fompeyrine, H. Siegwart, J.-P. Locquet, F. Nolting, S. Anders, E. E. Fullerton, et al., Science **287**, 1014 (2000).
[32] A. Scholl, F. Nolting, J. Stöhr, T. Regan, J. Lüning, J. W. Seo, J.-P. Locquet, J. Fompeyrine, S. Anders, H. Ohldag, et al., J. Appl. Phys. **11**, 7266 (2001).
[33] J. Lüning, F. Nolting, A. Scholl, H. Ohldag, J. W. Seo, J. Fompeyrine, J.-P. Locquet, and J. Stöhr, Phys. Rev. B **67**, 214433 (2003).
[34] J. Stöhr, A. Scholl, T. J. Regan, S. Anders, J. Lüning, M. R. Scheinfein, H. A. Padmore, and R. L. White, Phys. Rev. Lett. **83**, 1862 (1999).
[35] F. U. Hillebrecht, H. Ohldag, N. B. Weber, C. Bethke, U. Mick, M. Weiss, and J. Bahrdt, Phys. Rev. Lett. **86**, 3419 (2001).
[36] H. Ohldag, T. J. Regan, J. Stöhr, A. Scholl, F. Nolting, J. Lüning, C. Stamm, S. Anders, and R. L. White, Phys. Rev. Lett. **87**, 247201 (2001).
[37] H. Ohldag, A. Scholl, F. Nolting, S. Anders, F. U. Hillebrecht, and J. Stöhr, Phys. Rev. Lett. **86**, 2878 (2001).
[38] A. Scholl, M. Liberati, E. Arenholz, H. Ohldag, and J. Stöhr, Phys. Rev. Lett. **92**, 247201 (2004).
[39] M. Finazzi, A. Brambilla, P. Biagioni, J. Graf, G. Gweon, A. Scholl, A. Lanzara, and L. Duo, Phys. Rev. Lett. **97**, 097202 (2006).
[40] S. Krishnakumar, M. Liberati, C. Grazioli, M. Veronese, S. Turchini, P. Luches, S. Valeri, and C. Carbone, J. Magn. Magn. Mater. **310**, 8 (2007).
[41] I. P. Krug, F. U. Hillebrecht, M. W. Haverkort, A. Tanaka, L. H. Tjeng, H. Gomonay, A. Fraile-Rodriguez, F. Nolting, S. Cramm, and C. M. Schneider, Phys. Rev. B **78**, 064427 (2008).
[42] G. van der Laan and E. Arenholz, Eur. Phys. J. Special Topics **169**, 187 (2009).
[43] C. Boeglin, O. Ersen, M. Pilard, V. Speisser, and F. Kronast, Phys. Rev. B **80**, 035409 (2009).
[44] K. Arai, T. Okuda, A. Tanaka, M. Kotsugi, K. Fukumoto, M. Oura, Y. Senba, H. Ohashi, T. Nakamura, T. Matsushita, et al., J. Phys. Soc. Jpn **79**, 013703 (2010).
[45] G. van der Laan, Lect. Notes Phys. **697**, 143 (2006).
[46] G. van der Laan and I. W. Kirkman, J. Phys.:Condens. Matter **4**, 4189 (1992).
[47] W. L. Roth, Phys. Rev. **111**, 772 (1958).
[48] T. Yamada, J. Phys. Soc. Jpn **18**, 520 (1963).
[49] T. Yamada, J. Phys. Soc. Jpn **21**, 664 (1966).
[50] G. van der Laan, J. Magn. Magn. Mater. **192**, 297 (1999).
[51] E. Bauer, J. Phys.:Condens. Matter **13**, 11391 (2001).

LEGAL DISCLAIMER